Journal of Applied Physics

RESEARCH ARTICLE | MARCH 11 2015

Shock wave compression and release of hexagonal-close-packed metal single crystals: Inelastic deformation of *c*-axis magnesium FREE

J. M. Winey ; P. Renganathan; Y. M. Gupta

J. Appl. Phys. 117, 105903 (2015)
https://doi.org/10.1063/1.4914525

AIP Publishing

Shock wave compression and release of hexagonal-close-packed metal single crystals: Inelastic deformation of *c*-axis magnesium

J. M. Winey,[1,a)] P. Renganathan,[1,2] and Y. M. Gupta[1,3]
[1]*Institute for Shock Physics, Washington State University, Pullman, Washington 99164, USA*
[2]*School of Mechanical and Materials Engineering, Washington State University, Pullman, Washington 99164, USA*
[3]*Department of Physics and Astronomy, Washington State University, Pullman, Washington 99164, USA*

(Received 24 January 2015; accepted 28 February 2015; published online 11 March 2015)

To understand inelastic deformation mechanisms for shocked hexagonal-close-packed (hcp) metals, shock compression and release wave profiles, previously unavailable for hcp single crystals, were measured for *c*-axis magnesium crystals. The results show that the elastic-inelastic loading response is strongly time-dependent. Measured release wave profiles showed distinct peaked features, which are unusual for inelastic deformation during unloading of shocked metals. Numerical simulations show that pyramidal slip provides a reasonably good description of the inelastic loading response. However, $\{10\bar{1}2\}$ twinning is needed to explain the unloading response. The results and analysis presented here provide insight into the relative roles of dislocation slip and deformation twinning in the response of shocked hcp metals. © *2015 AIP Publishing LLC*.
[http://dx.doi.org/10.1063/1.4914525]

I. INTRODUCTION

The lower crystal symmetry of hexagonal-close-packed (hcp) metals, compared to cubic metals, results in a significantly more complex inelastic deformation response[1–3] that is challenging to understand and to model under dynamic high stress or shock wave loading conditions. Although hcp single crystal studies have long been used to provide insight into the inelastic deformation mechanisms arising under quasi-static loading,[4,5] the shock wave response of hcp single crystals has received only limited attention.[6–11] However, a recent study on shocked beryllium single crystals[12] has demonstrated that wave profile measurements for hcp single crystals shocked along different orientations, together with rigorous wave analysis using an anisotropic material modeling framework, can provide significant insight into inelastic deformation mechanisms in hcp metals.

Because twinning is an important inelastic deformation mechanism for hcp metals,[1–3] distinguishing between dislocation slip and deformation twinning in wave profiles measured for shocked hcp single crystals is an important need. Experiments that involve reversal of the mechanical load provide a potentially useful approach to address this need because twinning is unidirectional with respect to the sign of the shear deformation, whereas dislocation slip is bidirectional.[13] Shock wave compression, followed by stress release, provides a convenient approach for achieving load reversal in shocked solids because unloading from the peak state reverses the stress deviators, even though the mean stress remains compressive.[14] In previous experiments on zinc[9,10] and magnesium[11] single crystals, the samples were subjected to shock compression, followed by tensile loading to failure (spall). However, due to the configuration used in these experiments, the wave profile features related to the unloading response were obscured by the features related to the spall event. Therefore, measured wave profiles from well characterized load reversal experiments are currently unavailable for shocked hcp metal single crystals.

We have addressed this need by measuring wave profiles for shock wave compression and release of *c*-axis magnesium (Mg) single crystals in plate impact experiments. The measured profiles, together with numerical simulations using an anisotropic modeling framework,[12,15] have provided significant insight into the inelastic deformation mechanisms for shocked Mg crystals, including the relative roles of dislocation slip and deformation twinning in determining the observed inelastic deformation response.

II. EXPERIMENTAL METHODS

The Mg samples (99.999% pure) used in the experiments were cut from single crystal boules obtained from Metal Crystals and Oxides, Ltd. (Cambridge, UK) and were oriented to within 2° of the *c*-axis using *x*-ray Laue diffraction. The surfaces were ground flat and polished by hand using diamond suspensions (down to 1 μm particle size) on paper. The Mg sample thicknesses are shown in Table I. The Mg samples were bonded to a *z*-cut quartz buffer (0.125 in. thickness) and a fused silica optical window (0.375 in. thickness). Prior to bonding, aluminum mirrors were deposited on the front of the fused silica window and on the back of the quartz buffer to enable laser interferometry measurements.[16]

Figure 1 shows a schematic view of the plate impact experimental configuration. Using a light gas gun, *a*-cut sapphire discs (0.125 in. thickness) were impacted on the quartz−Mg−fused silica targets. The measured impact velocities are shown in Table I. Upon impact, shock waves propagated into the quartz buffer and into the sapphire impactor. The shock wave in the quartz buffer was transmitted through the Mg sample and into the fused silica window.

a)Electronic mail: mwiney@wsu.edu

TABLE I. Summary of experiments.

Experiment number	Mg thickness (mm)	Impact velocity (m/s)	Elastic shock velocity (m/s)	Elastic wave interface velocity (m/s)	Elastic wave amplitude (GPa)	Peak stress (GPa)
1 (14-503)	1.797	474	6.17	0.0615	0.73	4.2
2 (14-504)	4.005	476	6.13	0.0522	0.66	4.2
3 (14-507)	2.002	304	6.17	0.0932	1.11	2.6

The shock wave in the sapphire impactor was reflected from the sapphire rear surface (left hand side in Fig. 1) and propagated back through the sapphire−quartz−Mg−fused silica system as a release wave. Because the different materials in the target and the impactor have different mechanical impedances, the longitudinal stress in the shocked Mg samples experienced only partial release within the time duration of the experiments.

Particle velocity histories were measured at the Mg sample−fused silica interface using a velocity interferometer system (VISAR).[16] In addition, velocity histories were measured at three locations at the back of the quartz buffer to enable determination of impact tilt. The elastic shock wave velocity in the Mg samples was determined from the measured shock wave arrival times at the front and back sample interfaces.

We note that the experiments described here differ from recently published experiments[11] on shocked Mg single crystals in two important ways: (1) The use of an optical window (fused silica) in the present experiments, in contrast to the Mg free surface measurements (no window) reported previously,[11] enables the unloading response of the Mg samples to be examined without being obscured by the spall response. (2) The impactor, buffer, and optical window materials used in the present experiments respond elastically for the peak stresses reported here, enabling the key wave profile features due to shock compression and release of the Mg single crystals to be distinguished easily and accurately.

III. RESULTS

Three plate impact experiments were conducted for shock compression and release of *c*-axis Mg single crystals (thicknesses ranging from 1.8 mm to 4.0 mm) at peak stresses of 2.6 GPa or 4.2 GPa (see Table I). The measured wave profiles at the Mg-fused silica interface are shown in Fig. 2. The profiles reveal a two-wave, elastic-plastic shock compression response, with sharply peaked elastic waves followed by significant stress relaxation. In addition, comparison of the profiles from the two 4.2 GPa experiments indicates elastic wave attenuation with propagation distance. These features are indicative of a strongly time-dependent elastic-inelastic response. Overall, the elastic wave features observed in our 4.2 GPa experiments are qualitatively consistent with the free surface measurements published recently.[11]

The elastic wave stress amplitudes, determined from the measured elastic wave interface velocities and the measured shock wave velocities, are shown in Table I. Although the elastic wave stress amplitudes for the 4.2 GPa experiments are roughly consistent with those reported previously,[11] Fig. 2 and Table I show that the elastic wave amplitude observed here for the 2.6 GPa experiment is significantly larger than that for the 4.2 GPa experiments. This result is surprising because the opposite peak stress dependence is typically expected based on time-dependent inelastic deformation mechanisms, such as dislocation motion.[17] Confirmation experiments (not shown here) have demonstrated that the larger elastic wave amplitude for the 2.6 GPa experiment is a reproducible phenomenon.

The measured release wave profiles for *c*-axis Mg single crystals, a key feature of our work, are also shown in Fig. 2. All of the release profiles show very distinct, peaked features

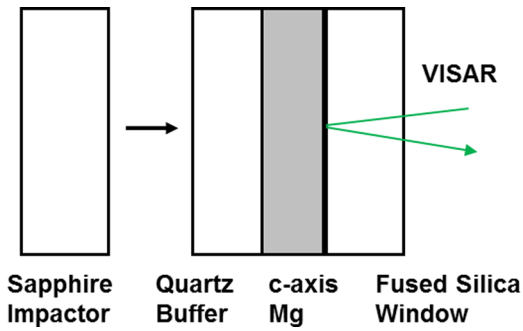

FIG. 1. Experimental configuration for measuring particle velocity profiles for shock compression and release in *c*-axis Mg single crystals. The histories were measured at the Mg-fused silica interface using a velocity interferometer system (VISAR) (Ref. 16). The left side of the sapphire impactor is a free surface.

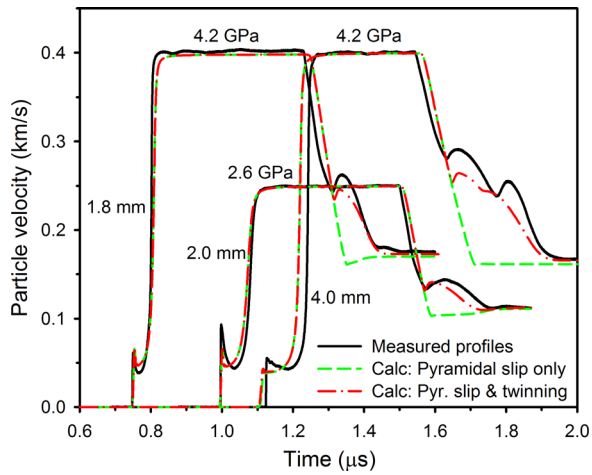

FIG. 2. Measured and calculated velocity histories at the sample-window interface for shock compression and release of c-axis Mg crystals. The black solid curves are the measured velocity histories. The remaining curves are calculations using the pyramidal slip only model (green dashed curves) or the pyramidal slip and $\{10\bar{1}2\}$ twinning models (red dotted-dashed curves). The wave profile for the 2.6 GPa experiment is shifted 0.2 μs to the right for visual clarity.

indicative of an elastic-inelastic unloading response. These distinct features are highly unusual for shocked metals; typically, the release wave features are indistinct and smeared out,[18] even for single crystals.[19]

IV. ANALYSIS AND DISCUSSION

Recent work on shocked beryllium[12] has shown that rigorous analysis of measured wave profiles, using numerical simulations, can provide significant insight into inelastic deformation mechanisms in shocked hcp metal single crystals. Hence, wave propagation simulations were carried out for shock compression and release of *c*-axis Mg single crystals for comparisons with the measured wave profiles. The anisotropic material modeling framework used in these simulations is similar to that used in the recent beryllium work; detailed descriptions have been published elsewhere.[12,15] Summarized briefly, the elastic response of Mg single crystals was described using measured second-order and third-order elastic constants[20] and calculated fourth-order elastic constants.[21] To determine inelastic strains, the rate of inelastic shear deformation ${}^{\alpha}\dot{\gamma}$ for each dislocation slip or twinning system α was determined from the resolved shear stress (RSS) ${}^{\alpha}\tau$ using micromechanical models.[12,15]

Calculated wave profiles from simulations incorporating pyramidal slip only and pyramidal slip together with $\{10\bar{1}2\}$ twinning are shown in Fig. 2. The calculations incorporating pyramidal slip only (green dashed curves) provide a good match to the compressive loading portion of the measured wave profiles for the 4.2 GPa experiments, including the elastic wave features. However, the calculations are unable to match the larger elastic wave amplitude observed in the 2.6 GPa experiment. In these calculations, significant strain hardening was incorporated in the pyramidal slip model to provide a good match to the second or the inelastic deformation wave and the measured peak particle velocity. For the unloading profiles, calculations using the pyramidal slip model provide a poor match to the measured results. The distinct release wave features corresponding to the elastic-inelastic unloading response are completely absent from the calculated profiles.

The red dotted-dashed curves in Fig. 2 are the wave profiles calculated by incorporating both pyramidal slip and $\{10\bar{1}2\}$ twinning models. Because $\{10\bar{1}2\}$ twinning in Mg single crystals is not activated for compressive loading along the *c*-axis,[1] the loading portion of the calculated wave profile is identical to that calculated using pyramidal slip only. However, in contrast to the pyramidal slip only, the combination of pyramidal slip and $\{10\bar{1}2\}$ twinning provides a good match to the measured unloading profile, including the distinct peaked features corresponding to inelastic deformation during unloading.

To better understand the results shown in Fig. 2, calculated stress histories determined at the center of the 4.0 mm thick Mg sample (expt. 2) are shown in Fig. 3. The stresses are expressed in a coordinate system where the longitudinal stress σ_{xx} is aligned with the wave propagation direction. Due to the six-fold rotational symmetry possessed by the Mg *c*-axis, the two calculated lateral stresses are equivalent.

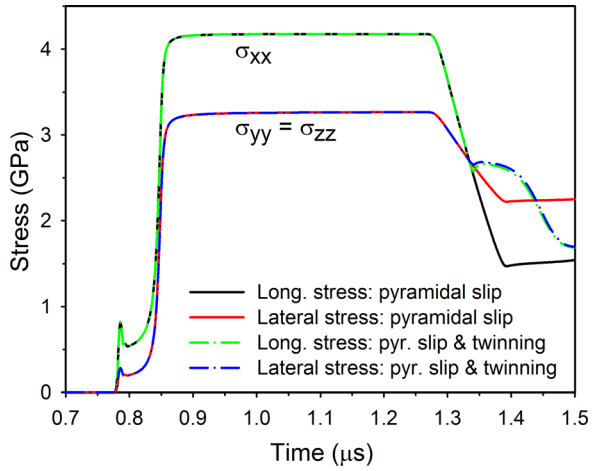

FIG. 3. Calculated stress histories at the sample center for shock compression and release of c-axis Mg crystals shocked to 4.2 GPa (expt. 2). The solid curves are calculations using the pyramidal slip only model. The dotted-dashed curves are calculations using the pyramidal slip and $\{10\bar{1}2\}$ twinning models.

Calculations using the pyramidal slip model (solid curves) reveal that the strain hardening incorporated in the model leads to large stress differences $\sigma_{xx} - \sigma_{yy}$ $(= \sigma_{xx} - \sigma_{zz})$ in the peak state of the shocked Mg samples. Upon the release wave arrival, the stress differences are reduced and, subsequently, undergo a sign change as the unloading progresses. However, because the stress differences obtained due to the partial stress release do not achieve the magnitude present in the peak state, pyramidal slip is not activated during unloading; and the calculated unloading response is completely elastic (the featureless unloading response shown in Fig. 2).

The stress histories calculated using the combination of pyramidal slip and $\{10\bar{1}2\}$ twinning models (dotted-dashed curves) are identical to those calculated using the pyramidal slip model until the stress differences change sign during unloading. After the sign reversal, the stress differences calculated using the combined pyramidal slip and twinning models remain small for the remainder of the release wave, due to stress relaxation resulting from the activation of $\{10\bar{1}2\}$ twinning.

The calculated RSS histories and the calculated inelastic shear strain histories, determined at the center of the 4.0 mm thick Mg sample (expt. 2) using the combined pyramidal slip and $\{10\bar{1}2\}$ twinning models, are shown in Figs. 4(a) and 4(b), respectively. Due to the six-fold rotational symmetry of the Mg *c*-axis, the histories for all pyramidal slip planes are the same, as are the histories for all $\{10\bar{1}2\}$ twinning planes. The calculated histories (Figs. 4(a) and 4(b)) show the onset of pyramidal slip at the peak of the elastic wave. Due to strain hardening, the RSS on the pyramidal slip planes continues to increase for loading beyond the elastic limit, reaching a maximum in the peak state.

During unloading, the sign change for the stress differences (Fig. 3) implies a reversal of the RSS on the dislocation slip and twinning planes, as shown in Fig. 4(a). Upon reversal, the RSS on the $\{10\bar{1}2\}$ planes becomes favorable for twinning; the calculated onset of twinning is indicated in Fig. 4(a). In Fig. 4(b), the inelastic shear strain due to

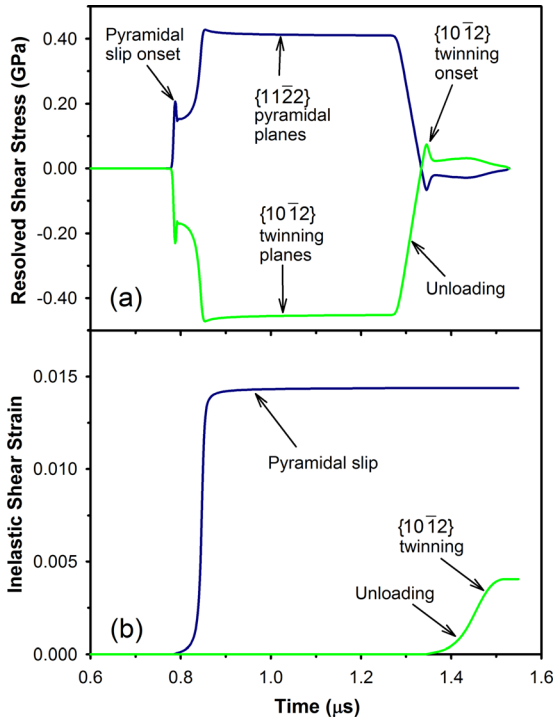

FIG. 4. Calculated histories at the sample center for shock compression and release of c-axis Mg crystals shocked to 4.2 GPa (expt. 2): (a) resolved shear stress; (b) inelastic shear strain. The calculations used the pyramidal slip and $\{10\bar{1}2\}$ twinning models.

pyramidal slip is much larger than that due to twinning because the Mg samples do not unload completely within the time duration of the experiments. Because the twinning shear for a $\{10\bar{1}2\}$ twin in Mg is 0.129,[1] the inelastic shear strain shown in Fig. 4(b) indicates that the twinned volume fraction after the partial unloading in these experiments is approximately 19%.

The above discussion has shown that pyramidal slip provides a reasonably good description of the inelastic response of shocked *c*-axis Mg. However, under quasi-static loading, inelastic deformation resulting from *c*-axis compression occurred primarily in thin bands oriented parallel to the $\{10\bar{1}1\}$ planes.[4,5] Based on earlier work,[22] these bands were interpreted in terms of a complex mechanism that involves $\{10\bar{1}1\}$ twinning, followed by retwinning on $\{10\bar{1}2\}$ planes within the twinned volume, followed by basal slip within the doubly twinned volume.[4,5] Due to the challenges involved in accurately modeling this complex inelastic deformation mechanism, no attempt was made to incorporate the same in the calculations presented here. However, the inability of the pyramidal slip model to match the large elastic wave amplitude observed for the 2.6 GPa experiment (Fig. 2) raises the question: Does the complex $\{10\bar{1}1\}$ twinning mechanism observed previously[4,5,22] play a significant role in the inelastic deformation response of shocked *c*-axis Mg single crystals?

V. CONCLUSIONS

The measured shock wave compression and release profiles presented here for Mg single crystals constitute the first reported examination of the load reversal response for a shocked hcp single crystal. Analysis of the wave profiles has provided significant insight into the inelastic deformation response. Our main findings include

(1) The measured elastic wave amplitudes are larger for smaller peak stresses, in contrast to expectations based on typical dislocation-based pictures of inelastic deformation.[17]
(2) Distinct elastic-inelastic release wave features were observed, which differ significantly from those observed previously for shocked metals.
(3) Results from numerical simulations show that incorporating pyramidal slip and $\{10\bar{1}2\}$ twinning provides a good overall description for both loading and unloading wave profiles. In particular, $\{10\bar{1}2\}$ twinning (not operative in compression) provides a good match to the distinct features observed in the release wave measurements.

The work presented here constitutes an important step in addressing a long-standing scientific question: What are the relative roles of dislocation slip and deformation twinning in determining the inelastic deformation response of shocked hcp metals? However, our findings also raise two interesting and important questions specific to shocked *c*-axis Mg: (1) How to understand the larger elastic wave amplitudes observed for lower peak stresses? (2) What is the role of $\{10\bar{1}1\}$ twinning in the inelastic deformation response of shocked c-axis Mg? Answers to these questions will likely require well characterized shock wave experiments, together with numerical simulations, on thin (<1 mm) *c*-axis Mg samples shocked to different peak stresses.

ACKNOWLEDGMENTS

N. Arganbright, B. Williams, and K. Zimmerman are thanked for their expert assistance with the experiments. K. Xie and K. Hemker are gratefully acknowledged for their assistance in characterizing residual surface damage in the Mg single crystal samples. This work was supported by the Army Research Laboratory (Cooperative Agreement No. W911NF-12-2-0022) and by the Department of Energy/NNSA (Cooperative Agreement No. DE-NA0000970).

[1]M. H. Yoo, Metall. Trans. A **12**, 409 (1981).
[2]R. E. Reed-Hill, *The Inhomogeneity of Plastic Deformation* (American Society for Metals, 1973).
[3]W. G. Hosford, *The Mechanics of Crystals and Textured Polycrystals* (Oxford University Press, 1993).
[4]B. C. Wonsiewicz and W. A. Backofen, Trans. AIME **239**, 1422 (1967).
[5]E. W. Kelley and W. F. Hosford, Trans. AIME **242**, 5 (1968).
[6]M. A. Mogilevskiy, Phys. Met. Metall. **28**, 130 (1969).
[7]P. L. Studt, E. Nidick, F. Uribe, and A. K. Mukherjee, in *Metallurgical Effects at High Strain Rates*, edited by R. W. Rohde, B. M. Butcher, J. R. Holland, and C. H. Karnes (Plenum, 1973), p. 379.
[8]L. E. Pope and J. N. Johnson, J. Appl. Phys. **46**, 720 (1975).
[9]A. A. Bogatch, G. I. Kanel, S. V. Razorenov, A. V. Utkin, S. G. Protasova, and V. G. Sursaeva, Phys. Solid State **40**, 1676 (1998).
[10]G. S. Bezruchko, G. I. Kanel, and S. V. Razorenov, Tech. Phys. **50**, 621 (2005).
[11]G. I. Kanel, G. V. Garkushin, A. S. Savinykh, S. V. Razorenov, T. de Resseguier, W. G. Proud, and M. R. Tyutin, J. Appl. Phys. **116**, 143504 (2014).
[12]J. M. Winey and Y. M. Gupta, J. Appl. Phys. **116**, 033505 (2014).

[13]M. V. Klassen-Neklyudova, *Mechanical Twinning of Crystals* (Consultants Bureau, 1964).
[14]G. R. Fowles, J. Appl. Phys. **32**, 1475 (1961).
[15]J. M. Winey and Y. M. Gupta, J. Appl. Phys. **99**, 023510 (2006).
[16]L. M. Barker and R. E. Hollenbach, J. Appl. Phys. **43**, 4669 (1972).
[17]Y. M. Gupta, J. Appl. Phys. **46**, 3395 (1975).
[18]J. M. Winey, J. N. Johnson, and Y. M. Gupta, J. Appl. Phys. **112**, 093509 (2012).
[19]H. Huang and J. R. Asay, J. Appl. Phys. **101**, 063550 (2007).
[20]E. R. Naimon, Phys. Rev. B **4**, 4291 (1971).
[21]R. R. Rao and A. Padmaja, J. Appl. Phys. **67**, 227 (1990).
[22]R. E. Reed-Hill, Trans. TMS-AIME **218**, 554 (1960).